Squirming inside a liquid droplet with surface viscosities

Herve Nganguia and Adedoyin Adegbuyi
Department of Mathematics, Towson University, Towson, Maryland 21252, USA

Matthew Uffenheimer and On Shun Pak[*]
Department of Mechanical Engineering, Santa Clara University, Santa Clara, California 95053, USA

The possibility of encapsulating therapeutic substances with active particles inside droplets, thereby propelling their motion from within, presents exciting opportunities for biomedical applications such as targeted drug delivery. In realistic biological and environmental settings, droplet interfaces often exhibit complex interfacial rheological behaviors due to different molecules or particles laden on the interface. Motivated by this complexity, we investigate the effects of interfacial rheology on the motion of an active droplet consisting of a liquid droplet enclosing an active particle described by the squirmer model. Specifically, we examine theoretically how surface shear and dilatational viscosities impact the propulsion of both the enclosed squirmer and the enclosing droplet. Our results indicate that while surface shear viscosity has no impact on the propulsion speeds, both the droplet and the squirmer swim slower with increased surface dilatational viscosity. The independence of propulsion speeds from surface shear viscosity is a feature shared with the classical problem of a translating droplet with surface viscosities. However, we add a cautionary remark on the subtlety in interpreting the impact of surface viscosities in these two problems. We also examine how the presence of surface viscosities affects the flow field and energetic cost in this active droplet system. These findings represent a first step towards understanding how complexities arising from realistic biological or environmental settings influence the behavior of microswimmer-driven droplets, paving the way for their potential applications in these complex environments.

I. INTRODUCTION

Emulsion droplets have emerged as promising platforms in droplet microfluidics, serving as microcompartments for chemical and biological reactions [1,2]. In particular, the ability to encapsulate living cells within droplets offers a precise and controlled microenvironment for conducting high-throughput, cell-based assays [3,4]. Recently, the encapsulation of motile cells, such as the nematode *Caenorhabditis elegans* [5,6], within droplets has sparked inquiries into the potential for inducing motion of the encapsulating droplet by the active particles it contains. Beyond biological cells, the development of artificial microswimmers has attracted substantial attention in recent decades for their potential biomedical and environmental applications [7–12]. The possibility of encapsulating therapeutic substances with artificial microswimmers within a droplet, propelling its motion from within, therefore opens up exciting opportunities for their utilization in drug delivery and related applications.

---

[*]Contact author: opak@scu.edu

In previous experiments where nematodes [5,6] and magnetically rotated helical micropropellers [13] were enclosed within droplets, the encapsulating droplets were not observed to be motile. The lack of observable droplet motion has been attributed to the droplets being anchored due to the constraints of microfluidic setups or the relatively small size of the swimmer in comparison to the droplet. A combined theoretical and numerical study by Reigh *et al.* [14] showed that a spherical squirmer enclosed in a droplet of comparable size is able to propel the droplet. The swimming motion of the squirmer is impacted by the confinement effect due to the fluid-fluid interface of the droplet, which moves at a speed depending on the surface velocity distribution on the squirmer. It was shown that the droplet always moves slower than a squirmer with tangential surface velocities, whereas a squirmer with both tangential and radial surface velocities is able to attain the same swimming speed as the droplet, maintaining a concentric configuration in their coswimming state. A later analysis based on a collection of point forces inside the droplet [15] also demonstrated the ability of generating droplet propulsion through internal active devices. In addition, the effect of an imposed shear flow on the deformation dynamics of a droplet encapsulating a model microswimmer has also been considered theoretically [16].

In many naturally occurring and industrial scenarios, the fluid-fluid interfaces, however, are often laden with different molecules or particles. These complex interfaces display various interfacial behaviors beyond what a single value of surface tension can describe [17–19]. It is therefore of interest to examine how various complex interfacial behaviors affect the motion of active droplets. In particular, Shaik *et al.* [20] investigated how Marangoni stresses due to surfactant concentration inhomogeneities influence the locomotion inside a surfactant-laden drop. Another mechanism the contaminants can affect the interfacial behavior is through the generation of interfacial viscous stresses. The movement of the contaminants on the interface can cause shear and dilatational friction, characterized by surface viscosities, leading to additional resistance to shear and dilatational deformations of the interface [17–19]. More recently, Sprenger *et al.* [21] presented a first analysis on how interfacial rheology affects the motion of an active droplet enclosing a swimmer. Specifically, the study focuses on the effect of surface shear viscosity and represents the encapsulated particle as different flow singularities inside the droplet. A similar approach was also employed to investigate the motion of a swimming microorganism modeled as a Stokes dipole outside a droplet with surface shear viscosity [22].

In this work, we extend previous studies by investigating the effect of both surface shear and dilatational viscous stresses on the motion of a liquid droplet enclosing an active particle modeled as a squirmer [23–26]. The squirmer model allows us to consider swimmers of finite sizes and examine how geometrical factors influence the propulsion behaviors. Furthermore, the treatment via Lamb's general solution [27,28] allows us to obtain exact, analytical results for the problem. Our results have elucidated individual and combined effects of surface shear and dilatational viscosities on the swimming kinematics and energetics as well as the flows surrounding the active droplet and the enclosed swimmer. The exact solutions presented here will also be useful for validating subsequent numerical treatments of related problems.

The remainder of the paper is structured as follows. We formulate the problem in Sec. II, presenting the governing equations, boundary conditions, and solution method. In Sec. III, we discuss the results on the propulsion speeds of the squirmer and the droplet (Sec. III A), their surrounding flows (Sec. III B), and the energetic cost (Sec. III C) of squirming inside a drop with surface viscosities. We also highlight the subtlety in interpreting the impact of surface viscosities on squirming inside a liquid droplet, before some concluding remarks in Sec. IV.

II. PROBLEM FORMULATION

A. Governing equations and boundary conditions

We consider a spherical squirmer with a distribution of tangential surface velocity [23–26], $\mathbf{u}_{sq} = \sum_{n=1}^{\infty} B_n V_n(\cos\theta)\mathbf{e}_\theta$, where $V_n = -2P_n^1(\cos\theta)/[n(n+1)]$ and $P_n^1(\cos\theta)$ are the associated
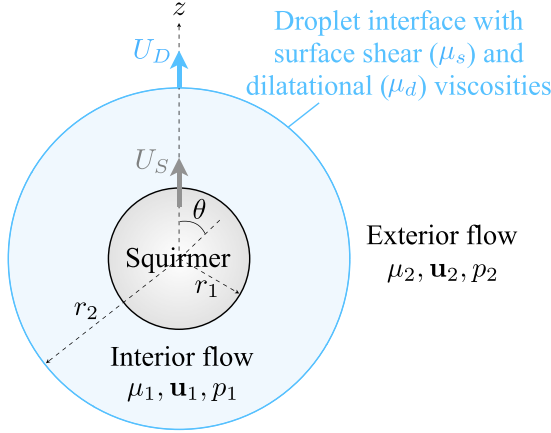
FIG. 1. A spherical squirmer with radius r_1 is enclosed concentrically within a spherical droplet with radius r_2. The squirming motion generates a flow $(\mathbf{u}_1, p_1)$ in the interior fluid with viscosity μ_1 and a flow $(\mathbf{u}_2, p_2)$ in the exterior fluid with viscosity μ_2. The droplet interface is characterized with both surface shear (μ_s) and dilatational (μ_d) viscosities, modeled by the Boussinesq-Scriven constitutive equation. The unknown propulsion speeds of the squirmer and the droplet are denoted as U_S and U_D, respectively.

Legendre polynomials of the first kind. In an unbounded Stokes flow, the B_1 mode is associated with a source dipole and is the only mode contributing to swimming, whereas the B_2 mode is associated with a force dipole. Therefore, only the first two modes are typically considered in locomotion problems and their relative signs can be adjusted to represent a puller ($B_2/B_1 > 0$; e.g., the alga *Chlamydomonas*), a pusher ($B_2/B_1 < 0$; e.g., the bacterium *Escherichia coli*), or a neutral squirmer ($B_2/B_1 = 0$). Here, we focus our analysis on a squirmer of radius r_1 with the first two tangential squirming modes,

$$\mathbf{u}_{\mathrm{sq}} = [\bar{B}_1 \sin\theta + (\bar{B}_2/2)\sin 2\theta]\mathbf{e}_\theta, \tag{1}$$

enclosed in a spherical droplet of radius r_2 in a concentric configuration, as illustrated in Fig. 1. The effect due to a radial squirming motion is discussed in Appendix B. The surface tension on the drop is assumed to be sufficiently large so that the drop remains spherical in shape in the low capillary number regime. Under this geometric configuration, due to axisymmetry, the squirmer and the droplet both propel along the z direction with velocities $\mathbf{U}_S = U_S\mathbf{e}_z$ and $\mathbf{U}_D = U_D\mathbf{e}_z$, respectively, but their magnitudes are generally different ($U_S \neq U_D$). The fluids inside and outside the droplet are Newtonian with the interior and exterior dynamic viscosities denoted as μ_1 and μ_2, respectively. The incompressible flow inside and outside the droplet, therefore, satisfy the Stokes equations,

$$-\nabla p_j + \mu_j \nabla^2 \mathbf{u}_j = \mathbf{0}, \quad \nabla \cdot \mathbf{u}_j = 0, \tag{2}$$

where p_j are the pressure fields and $\mathbf{u}_j$ are the velocity fields interior ($j = 1$) and exterior ($j = 2$) to the droplet. We consider the problem in the laboratory frame, where the velocity in the far field decays to zero, $\mathbf{u}_2(r \to \infty) = \mathbf{0}$. On the squirmer's surface ($r = r_1$), the velocity is given by a combination of the prescribed squirming velocity and the unknown propulsion velocity,

$$\mathbf{u}_1 = \mathbf{u}_{\mathrm{sq}} + \mathbf{U}_S. \tag{3}$$

On the droplet interface ($r = r_2$), the tangential and and normal velocities are continuous,

$$\mathbf{u}_1 \cdot \mathbf{t} = \mathbf{u}_2 \cdot \mathbf{t}, \tag{4}$$

$$\mathbf{u}_1 \cdot \mathbf{n} = \mathbf{u}_2 \cdot \mathbf{n} = U_D \cos\theta, \tag{5}$$

where **t** and **n** are the tangential and normal unit vectors, respectively. The stress balance at the interface is given by

$$(\mathbf{T}_2 - \mathbf{T}_1) \cdot \mathbf{n} = -\nabla_s \cdot \boldsymbol{\tau}_s, \tag{6}$$

where $\mathbf{T}_j = -p_j \mathbf{I} + \mu_j [\nabla \mathbf{u}_j + (\nabla \mathbf{u}_j)^T]$ is the fluid stress tensor, $\nabla_s = \mathbf{P} \cdot \nabla$ is the surface gradient operator, and $\mathbf{P} = \mathbf{I} - \mathbf{nn}$ is the surface projection tensor. Here, the jump in traction is balanced by surface tension and interfacial stresses, modeled by the Boussinesq-Scriven constitutive equation [29] as

$$\boldsymbol{\tau}_s = \gamma \mathbf{P} + (\mu_d - \mu_s)(\nabla_s \cdot \mathbf{u}_s)\mathbf{P} + 2\mu_s \mathbf{D}_s, \tag{7}$$

where γ is the surface tension, μ_d is the surface dilatational viscosity, μ_s is the surface shear viscosity, $\mathbf{u}_s$ is the velocity on the droplet surface, and $\mathbf{D}_s = \{\mathbf{P} \cdot [\nabla_s \mathbf{u}_s + (\nabla_s \mathbf{u}_s)^T] \cdot \mathbf{P}\}/2$ is the surface rate of the deformation tensor. In the regime of small capillary numbers, where capillary forces dominate over viscous forces that tend to deform the drop, slight deviations from a spherical shape generate sufficient variations in curvature to satisfy the normal stress balance over the drop surface. Thus, the drop remains approximately spherical in this regime. Within the framework of domain perturbations, a spherical drop shape is prescribed as the leading-order approximation. In this case, the far-field condition, the tangential velocity continuity [Eq. (4)], and the kinematic boundary condition describing the rigid body motion of the spherical drop [Eq. (5)], along with the tangential stress balance in Eq. (6), are sufficient to fully determine the leading-order velocity and pressure fields. The normal stress balance in Eq. (6) can then be used to compute the next-order approximation to the drop shape in the domain perturbation technique [30,31].

We nondimensionalize lengths by the radius of the squirmer r_1, velocities by the first swimming mode $\bar{B}_1$, and stresses by $\mu_2 \bar{B}_1 / r_1$. Upon nondimensionalization of the governing equations and boundary conditions, relevant dimensionless groups emerge: First, the ratio $\beta = \bar{B}_2 / \bar{B}_1$ characterizes the relative strength of the second swimming mode relative to the first mode. Second, the geometric ratio $b = r_2 / r_1$ measures the size of the droplet relative to that of the enclosed squirmer. Third, the viscosity contrast $\lambda = \mu_1 / \mu_2$ compares the dynamic viscosity of the interior fluid to that of the exterior fluid. Finally, the dilatational Boussinesq number $\mathrm{Bq}_d = \mu_d / (\mu_2 r_1)$ and shear Boussinesq number $\mathrm{Bq}_s = \mu_s / (\mu_2 r_1)$ emerge, comparing the relative strength of different interfacial viscous stresses with the bulk viscous stress. Hereafter, we refer only to dimensionless quantities and use the same symbols as their dimensional counterparts for convenience.

B. Solution method: Lamb's general solution

We obtain the solution to the Stokes equations, Eqs. (2), via Lamb's general solution [14,28,32,33]. For this axisymmetric problem, the general solution of the velocity field in spherical coordinates is denoted as $\mathbf{u}_j = u_{r,j}\mathbf{e}_r + u_{\theta,j}\mathbf{e}_\theta$. The velocity field of the interior flow ($j = 1$) is expressed as [34,35]

$$u_{r,1} = \sum_{n=0}^{\infty} \left(A_n r^{n+1} + B_n r^{n-1} + \frac{C_n}{r^n} + \frac{D_n}{r^{n+2}} \right) P_n(\cos\theta), \tag{8}$$

$$u_{\theta,1} = \sum_{n=1}^{\infty} \left(-\frac{n+3}{2}A_n r^{n+1} - \frac{n+1}{2}B_n r^{n-1} + \frac{n-2}{2}\frac{C_n}{r^n} + \frac{n}{2}\frac{D_n}{r^{n+2}} \right) V_n(\cos\theta), \tag{9}$$

whereas the velocity field of the exterior flow ($j = 2$) is expressed as

$$u_{r,2} = \sum_{n=0}^{\infty} \left(G_n r^{n+1} + H_n r^{n-1} + \frac{E_n}{r^n} + \frac{F_n}{r^{n+2}} \right) P_n(\cos\theta), \tag{10}$$

$$u_{\theta,2} = \sum_{n=1}^{\infty} \left(-\frac{n+3}{2}G_n r^{n+1} - \frac{n+1}{2}H_n r^{n-1} + \frac{n-2}{2}\frac{E_n}{r^n} + \frac{n}{2}\frac{F_n}{r^{n+2}} \right) V_n(\cos\theta). \tag{11}$$

Here, $P_n(\cos\theta)$ is the Legendre polynomial of degree n. The unknown coefficients A_n, B_n, C_n, D_n, E_n, F_n, G_n, and H_n are to be determined by boundary conditions in the problem. The far-field condition of a quiescent flow requires that $G_n = H_n = 0$. The velocity distribution on the squirmer surface, Eq. (3), requires

$$u_{r,1}(r = 1) = U_S \cos\theta, \tag{12}$$

$$u_{\theta,1}(r = 1) = (1 - U_S)\sin\theta + \frac{\beta}{2}\sin(2\theta), \tag{13}$$

whereas the continuity of the tangential and normal velocities on the droplet surface, Eqs. (4) and (5), requires

$$u_{r,1}(r = b) = u_{r,2}(r = b), \tag{14}$$

$$u_{r,1}(r = b) = U_D \cos\theta, \tag{15}$$

$$u_{\theta,1}(r = b) = u_{\theta,2}(r = b). \tag{16}$$

Finally, the tangential component of the stress balance at the interface ($r = b$) given by Eq. (6),

$$T_{r\theta,2} - T_{r\theta,1} = -\frac{1}{b^2}\left[2\mathrm{Bq}_s u_\theta + (\mathrm{Bq}_d + \mathrm{Bq}_s)\frac{\partial}{\partial\theta}\left[\frac{1}{\sin\theta}\frac{\partial}{\partial\theta}(u_\theta\sin\theta)\right] + 2\mathrm{Bq}_d\frac{\partial u_r}{\partial\theta}\right], \tag{17}$$

provides the remaining equation required to determine the unknown coefficients in the system in terms of the propulsion speeds of the squirmer, U_S, and droplet, U_D. The unknown propulsion speeds are then determined by applying the force-free condition on the surfaces of the squirmer (S_1) and the droplet (S_2):

$$\int_{S_1} \mathbf{T}_1 \cdot \mathbf{n}\,\mathrm{dS} = \int_{S_2} \mathbf{T}_2 \cdot \mathbf{n}\,\mathrm{dS} = \mathbf{0}. \tag{18}$$

III. RESULTS AND DISCUSSION

A. Propulsion speeds

By applying the method via Lamb's general solution described in Sec. II B, the propulsion speed of the enclosed squirmer is given by

$$U_S = \frac{2(2b^5 - 5b^2 + 3)\mathrm{Bq}_d + 2b[b^5(3\lambda + 2) + (5b^2 - 3)(\lambda - 1)]}{b^6(9\lambda + 6) + 6(b^5 - 1)\mathrm{Bq}_d + 6b(\lambda - 1)}, \tag{19}$$

whereas the speed of the enclosing droplet is given by

$$U_D = \frac{10b^3\lambda}{b^6(9\lambda + 6) + 6(b^5 - 1)\mathrm{Bq}_d + 6b(\lambda - 1)}. \tag{20}$$

We discuss several features of the propulsion speeds of the squirmer and the droplet. Firstly, similar to the case of an unbounded squirmer, the propulsion speeds are independent of β, meaning that only the $\bar{B}_1$ mode contributes to the propulsion of the squirmer and the droplet. Pushers and pullers ($\bar{B}_2 \neq 0$) have the same speed as the corresponding neutral squirmer ($\bar{B}_2 = 0$). Secondly, the propulsion speeds reduce to the results by Reigh *et al.* [14] for an enclosing clean drop without surface viscosity in the limit of $\mathrm{Bq}_s = \mathrm{Bq}_d = 0$. In addition, it is observed that the propulsion speeds only depend on the surface dilatational viscosity through Bq_d, independent of the surface shear viscosity (Bq_s). Such a feature is also observed in the classical problem of a translating droplet with surface viscosities [36,37], where the translational speed only depends on the surface dilatational viscosity and the surface shear viscosity is unimportant [38]. When the surface dilatational viscosity increases (i.e., increasing Bq_d), both the swimming speed of the enclosed squirmer and the speed of the enclosing
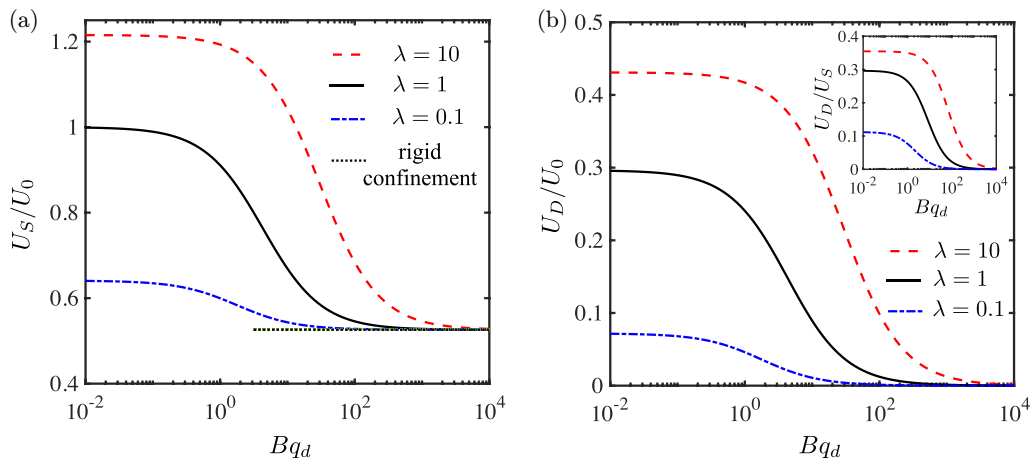
FIG. 2. Propulsion speeds of (a) the enclosed squirmer and (b) the enclosing drop, scaled by the propulsion speed of a squirmer $U_0 = 2/3$ in an unbounded fluid, as a function of Bq_d for different values of viscosity ratio, λ. The dotted line in (a) denotes the result in the limit of squirming under spherical rigid confinement [34]. Inset in (b) displays the ratio of the propulsion speed of the squirmer to that of the drop. In all cases, $b = 1.5$.

drop decrease monotonically as shown in Figs. 2(a) and 2(b), respectively. This qualitative feature remains the same across different regimes of viscosity contrast shown in Fig. 2 ($\lambda < 1$, $\lambda = 1$, and $\lambda > 1$). In the limit of $\mathrm{Bq}_d \to \infty$, the surface dilatational viscosity immobilizes the interface, effectively rendering it similar to a rigid confinement. The results therefore reduce to the motion of a squirmer under rigid spherical confinement [34], where $U_S \to (2b^5 - 5b^2 + 3)/[3(b^5 - 1)]$ [black dotted line, Fig. 2(a)] and $U_D \to 0$ [Fig. 2(b)]. As a remark, the inset of Fig. 2(b) shows that the squirmer always swims faster than its enclosing droplet in the concentric configuration, $U_D/U_S < 1$, for all values of Bq_d. We verify in Fig. 3 that this feature holds for different values of viscosity ratio λ and the relative size of the droplet b considered in this work.
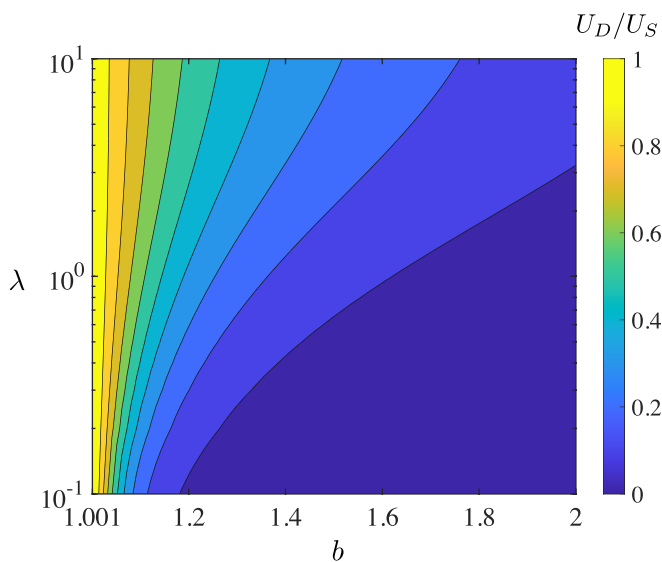

FIG. 3. The ratio of the propulsion speed of the squirmer to that of the droplet (U_D/U_S) as a function of the viscosity ratio (λ) and the relative size of the droplet (b). Here $\mathrm{Bq}_d = 10$.
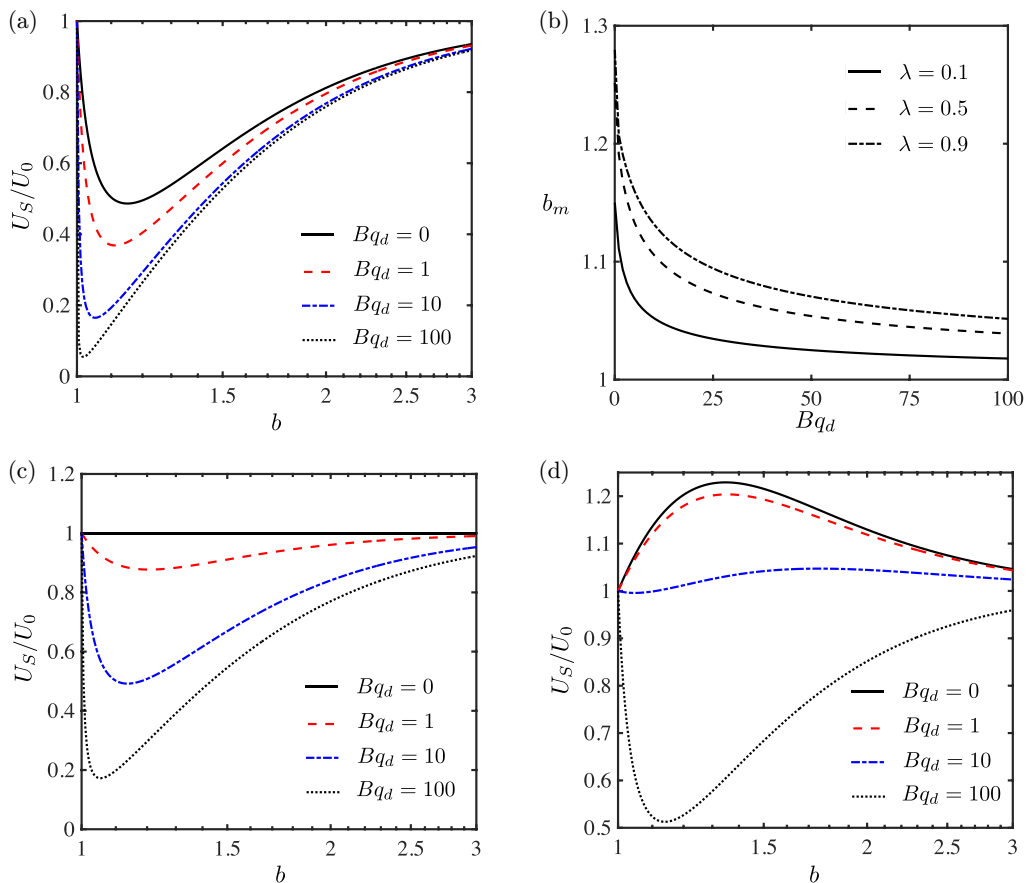
FIG. 4. Scaled propulsion speed of the squirmer as a function of the relative size of the droplet for different values of Bq_d (see legends) when (a) $\lambda = 0.1$, (c) $\lambda = 1$, and (d) $\lambda = 10$. Panel (b) displays the relative size of the droplet to the squirmer at which the local minimum of the scaled propulsion speed occurs (b_m) as a function of Bq_d for various values of $\lambda < 1$.

We further contrast the impacts of surface viscosities on this active droplet system with those on the classical translating droplet problem [36–38]. As previously mentioned, a key similarity in both problems is that the translational speed of the droplets (and the enclosed squirmer in the active droplet problem) depends solely on the surface dilatational viscosity, with no influence from the surface shear viscosity. However, we also observe a qualitatively distinct feature between the two scenarios. In the translating droplet problem, the motion of the droplet with surface viscosities is equivalent to that of a clean drop with a modified interior viscosity (in dimensional terms) $\mu_1^* = \mu_1 + 2\mu_d/(3r_2)$. Thus, the effect of surface (dilatational) viscosity may be understood as an equivalent increase in the interior viscosity in the translating droplet problem. However, neither the quantitative transformation nor the qualitative understanding applies to the active droplet problem. As shown in Fig. 2, increasing the interior viscosity (higher λ) enhances the propulsion speeds of both the active droplet and the squirmer. In contrast, increasing the surface dilatational viscosity (higher Bq_d) reduces their speeds. Therefore, the impact of surface viscosity in the active droplet problem cannot be understood as an effective increase in interior viscosity, as it is in the classical translating droplet problem.

Next, we examine how the propulsion speed of the squirmer varies with the relative size of the droplet at different values of Bq_d in Fig. 4. The system displays qualitatively different

characteristics depending on the regime of viscosity ratio. When $\lambda < 1$ (e.g., $\lambda = 0.1$), the enclosed squirmer generally propels at a speed less than its unbounded speed ($U_S/U_0 < 1$) for all values of b shown in Fig. 4(a), exhibiting a local minimum for different values of Bq_d. The presence of the surface dilatational viscosity ($\mathrm{Bq}_d > 1$) does not alter this feature qualitatively but consistently reduces the propulsion speed as Bq_d increases. In addition, Fig. 4(b) shows that the local minimum of the propulsion speed shifts to smaller values of b as Bq_d increases for different small viscosity contrasts ($\lambda < 1$). When the interior and exterior viscosities are the same ($\lambda = 1$), the squirmer propels at its unbounded speed ($U_S/U_0 = 1$) in the absence of surface viscosity [$\mathrm{Bq}_d = 0$; Fig. 4(c)]. With surface dilatational viscosity ($\mathrm{Bq}_d > 0$), the propulsion speed consistently decreases and a local minimum emerges, similar to the behavior observed in the $\lambda < 1$ regime [Fig. 4(a)]. Finally, when $\lambda > 1$ (e.g., $\lambda = 10$), in contrast to the speed variation observed for $\lambda < 1$, the enclosed squirmer always propels at a speed faster than its unbounded speed ($U_S/U_0 > 1$) when there is no surface viscosity ($\mathrm{Bq}_d = 0$), exhibiting a local maximum as shown in Fig. 4(d). When the interfacial viscous effect is relatively weak ($\mathrm{Bq}_d = 1$), the inclusion of surface dilatational viscosity consistently reduces the propulsion speed without altering the qualitative behavior. However, with a stronger interfacial viscous effect ($\mathrm{Bq}_d = 100$), there is a qualitative change in the speed variation with b. This stronger effect substantially reduces the propulsion speed to below the unbounded speed and induces a local minimum, rather than a maximum, in the variation.

B. Flow field

We utilize the analytical solution to examine the velocity field interior and exterior to the droplet. The coefficients in the velocity field generated by a neutral squirmer, $\mathbf{u}_j^{\bar{B}_1}$, are given by Eq. (A1) in Appendix A.

For a pusher ($\beta < 0$) or puller ($\beta > 0$), we can decompose the velocity field as $\mathbf{u}_j = \mathbf{u}_j^{\bar{B}_1} + \beta \mathbf{u}_j^{\bar{B}_2}$, where $\mathbf{u}_j^{\bar{B}_2}$ is the contribution from the $\bar{B}_2$ mode. The coefficients in $\mathbf{u}_j^{\bar{B}_2}$ are given by Eq. (A2) in Appendix A.

We discuss several features of the velocity field. Firstly, not only are the propulsion speeds of the droplet and the squirmer independent of the surface shear viscosity, but Eqs. (A1) show that the velocity field around a neutral squirmer ($\bar{B}_1$ mode) is also unaffected by surface shear viscosity, depending solely on the surface dilatational viscosity. Secondly, unlike the $\bar{B}_1$ mode flow around a neutral squirmer, the presence of surface shear viscosity does affect the flow around a pusher/puller (the $\bar{B}_2$ mode), as indicated by Eqs. (A2). Furthermore, the analytical expressions reveal that the dependence of the velocity field on surface viscosities always appears through the combined term $3\mathrm{Bq}_d + 2\mathrm{Bq}_s$, implying that surface shear and dilatational viscosities affect the flow around a pusher or puller in the same manner physically. Therefore, without loss of generality, we focus on visualizing the flow inside and outside drops with surface dilatational viscosities in Fig. 5; incorporating surface shear viscosities either has no effect (for the case of a neutral squirmer, $\beta = 0$) or leads to qualitatively the same effects to those observed with surface dilatational viscosities. In Fig. 5, we compare the flow patterns associated with droplets with (right sides, $\mathrm{Bq}_d = 100$) and without (left sides, $\mathrm{Bq}_d = 0$) surface dilatational viscosities. It is observed that the magnitude of the exterior flow is reduced for droplets with surface dilatational viscosities. This reduction is also evident from the coefficients in the exterior flows given by Eqs. (A1e) and (A1f) and Eqs. (A2e) and (A2f), which show a decrease in magnitude with increasing Bq_d. We also observe that the effects of surface dilatational viscosity on the flow pattern are most pronounced for intermediate values of β [e.g., $\beta = -1, -3$ in panels (b) and (c)]. For $\beta = 0$ [neutral squirmer, panel (a)] and a stronger pusher $\beta = -5$ [panel (d)], the flow patterns exhibit qualitatively similar features regardless of the presence of surface dilatational viscosities. We present only the flow patterns for pushers, as the flow patterns for pullers are qualitatively similar but inverted.
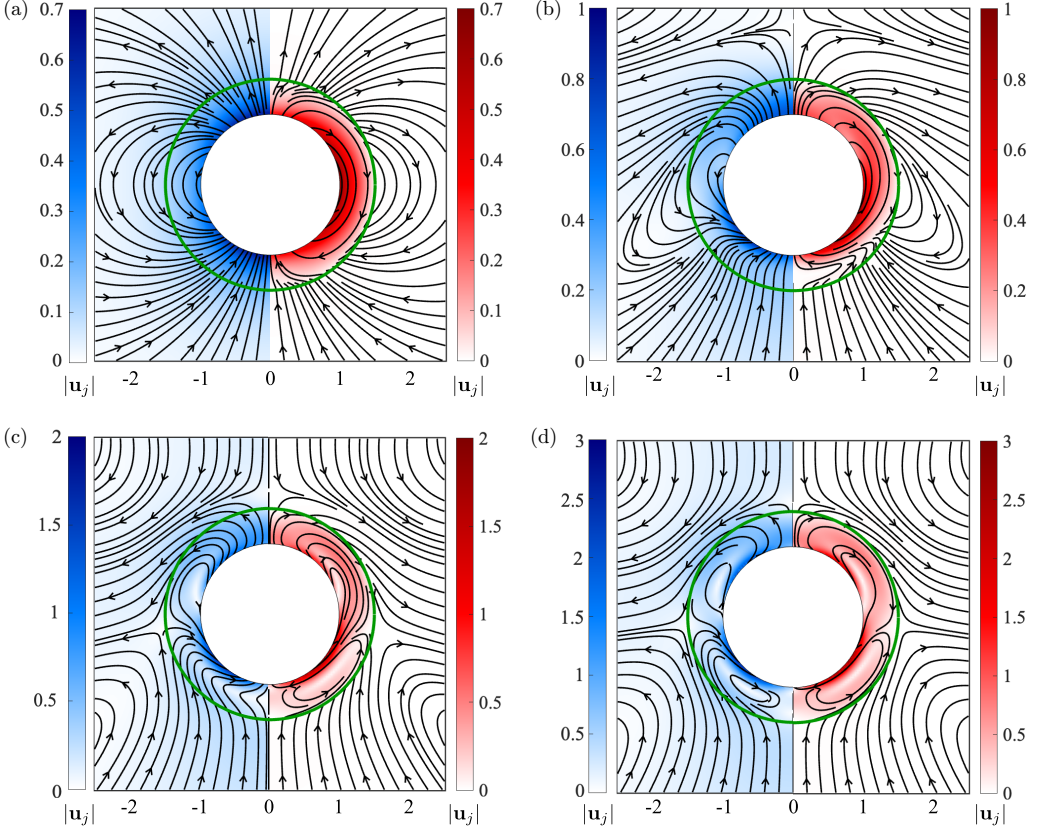
FIG. 5. The flow field inside and outside a liquid droplet (interface indicated by the green line) enclosing a squirmer with (a) $\beta = 0$, (b) $\beta = -1$, (c) $\beta = -3$, and (d) $\beta = -5$. In each panel, the left side (blue) displays the flow for a clean drop ($\mathrm{Bq}_d = 0$), whereas the right side (red) displays the flow for a drop with surface dilatational viscosity ($\mathrm{Bq}_d = 100$). In all cases, we set $\lambda = 1$, $b = 1.5$, and $\mathrm{Bq}_s = 0$. The colormap corresponds to the magnitude of the dimensionless velocity interior ($j = 1$) and exterior ($j = 2$) to the droplet.

We also examine the dependence of the velocity on the droplet interface, $\mathbf{u}(r = b) = \mathbf{u}_s$, on the surface viscosities. For a neutral squirmer, $\mathbf{u}_s^{\bar{B}_1} = u_{r,s}^{\bar{B}_1} \mathbf{e}_r + u_{\theta,s}^{\bar{B}_1} \mathbf{e}_\theta$, the normal and tangential components of the interfacial velocity are, respectively, given by

$$u_{r,s}^{\bar{B}_1} = U_D \cos\theta, \quad u_{\theta,s}^{\bar{B}_1} = \frac{F_1}{2b^3} \sin\theta. \tag{21}$$

For a pusher or puller, the interfacial velocity ($\mathbf{u}_s^{\bar{B}_1} + \beta \mathbf{u}_s^{\bar{B}_2}$) has the additional contribution $\mathbf{u}_s^{\bar{B}_2} = u_{r,s}^{\bar{B}_2} \mathbf{e}_r + u_{\theta,s}^{\bar{B}_2} \mathbf{e}_\theta$ due to the $\bar{B}_2$ mode, where

$$u_{r,s}^{\bar{B}_2} = 0, \quad u_{\theta,s}^{\bar{B}_1} = \frac{F_2}{b^4} \sin\theta \cos\theta. \tag{22}$$

We first remark that the normal component of the velocity in Eqs. (21) arises exclusively from the rigid body translation of the droplet at a speed of U_D. In other words, in a reference frame moving with the droplet, the interfacial velocity would be entirely tangential. Secondly, from the expressions of the coefficients F_1 [Eq. (A1f)] and F_2 [Eq. (A2f)], we observe from Eqs. (21) and (22) that the magnitude of the interfacial velocity reduces with increasing values of Bq_d (and Bq_s in the case of the $\bar{B}_2$ mode), as visualized in Fig. 6. This illustrates the effect of surface viscosities in immobilizing the droplet interface, approaching the limit of a rigid spherical boundary as $\mathrm{Bq}_d \to \infty$.
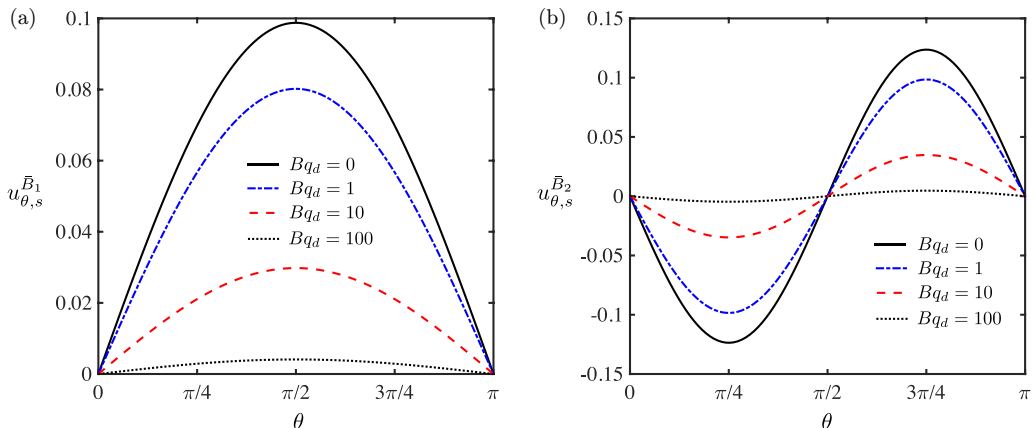
FIG. 6. Tangential interfacial velocity on the droplet due to the (a) $\bar{B}_1$ and (b) $\bar{B}_2$ modes for different values of Bq_d. In all cases, $b = 1.5$ and $\mathrm{Bq}_s = 0$.

C. Power consumption

We examine here the energetic cost associated with squirming inside a drop with surface viscosities. We calculate the power consumption, which is equal to the rate of work done by the squirming motion on the surface of the squirmer S, as

$$P = -\int_S \mathbf{T}_1 \cdot \mathbf{n} \cdot \mathbf{u}_1 \mathrm{d}S, \tag{23}$$

and display the results in Fig. 7 for a neutral squirmer [$\beta = 0$, panel (a)] and a pusher or puller [$\beta = \pm 3$, panel (b)]. For all cases considered in Fig. 7, the presence of surface viscosities (increasing Bq_d and/or Bq_s) leads to an increase in the power consumption by all squirmers, compared to the results for clean drops [14] (gray dotted lines). For neutral squirmers [Fig. 7(a)], since the flow field is independent of surface shear viscosity (Bq_s), the power consumption increases only
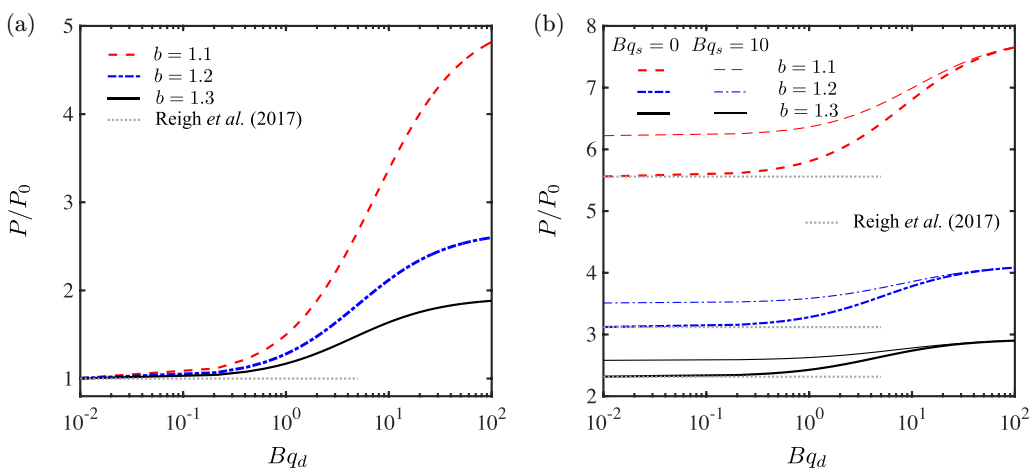

FIG. 7. Power consumption by the squirmer inside the droplet (P) scaled by the corresponding power consumed in an unbounded fluid (P_0) as a function of Bq_d for (a) $\beta = 0$ (neutral squirmer) and (b) $\beta = \pm 3$ (pusher or puller), under different relative sizes of the drop (see legends). The gray dotted lines represent the corresponding results for the clean droplet case ($\mathrm{Bq}_d = \mathrm{Bq}_s = 0$) given in Reigh *et al.* [14]. In all cases, $\lambda = 1$.

with the surface dilatational viscosity (Bq_d). For pushers and pullers [Fig. 7(b)], both surface shear and dilatational viscosities increase their power consumption. Since the surface shear and dilatational viscosities enter the flow field through the term $3Bq_d + 2Bq_s$, an increase in surface shear viscosity has physically the same impact on power consumption as an increase in surface dilatational viscosity. Figure 7(b) shows that as Bq_d increases, the effect of surface dilatational viscosity increasingly dominates over that of surface shear viscosity. Consequently, the curves corresponding to $Bq_s = 0$ (thicker lines) and $Bq_s = 10$ (thinner lines) converge as Bq_d becomes large.

Taken together, the results from Secs. III A and III C indicate that, compared to the case of a clean drop, a squirmer inside a drop with surface viscosities not only swims slower (Fig. 2) but also consumes more power (Fig. 7).

IV. CONCLUDING REMARKS

In this work, we explored the effects of surface viscosities on the motion of a liquid droplet enclosing a squirmer. Our study extends previous studies by incorporating both surface shear and dilatational viscosities, as well as considering swimmers of finite sizes, to uncover how these parameters influence swimming kinematics and energetics. The spherical and concentric geometric configuration of the problem setup allows exact, analytical results via Lamb's general solution. Our results indicate that the propulsion speeds of both the droplet and the enclosed squirmer are independent of surface shear viscosity, depending solely on surface dilatational viscosity. We note some measured values of surface dilatational viscosities [39], which can range from magnitudes on the order of 10^{-3} mN s m^{-1} for some interfaces with adsorbed low molecular weight surfactants [40] to 100 mN s m^{-1} or even larger for interfaces with adsorbed proteins [41,42], polymers [43,44], and lipids [45,46]. For an active particle with a size of $r_1 = 10$ μm and a bulk viscosity of $\mu_2 = 10^{-2}$ Pa s, the dilatational Boussinesq number can range as $Bq_d = O(10$–$10^6)$. In the high Bq_d regime, our results show a substantial reduction in the speed of the enclosing droplet, and the largely immobilized interface behaves similarly to rigid confinement. These findings suggest that deriving droplet propulsion from an enclosed active particle may not be an effective strategy in systems with high surface dilatational viscosities. In terms of the surrounding flows, surface shear viscosity does not impact the flow field generated by a neutral squirmer, whereas the combined effect of shear and dilatational viscosities (through the term $3Bq_d + 2Bq_s$) influences the flow generated by a pusher or puller. This latter feature implies that surface shear and diltational viscosities have the same physical impacts on the flow field and hence power consumption of the squirmer. Overall, the presence of surface viscosities leads to slower swimming speeds and higher power consumption for the squirmer compared to a clean droplet scenario.

We also compared our findings on the current active droplet problem with classical results on a translating droplet incorporating surface viscosities. Both problems share the feature that the translational speeds depend solely on the surface dilatational viscosity, not on the surface shear viscosity. In the classical translating droplet problem, the effect of surface viscosity can be effectively treated as an equivalent increase in interior viscosity. However, caution is needed when extending this notion to other problems, as it may lead to qualitatively different predictions, as illustrated by the example we provide here. Specifically, in our active droplet problem, while surface dilatational viscosity slows down both the enclosed squirmer and the enclosing droplet, an increase in interior viscosity actually leads to speed enhancement.

The exact solutions presented in this work can be employed for validating numerical simulations of related problems and can serve as a benchmark for future studies. We remark on several potential extensions of our work. Firstly, the concentric configuration considered here demonstrates that the droplet and the squirmer exhibit different speeds, which generally results in eccentric configurations as the swimming motion evolves. Analytical treatments using bispherical coordinates and numerical simulations are currently underway to examine whether the main features revealed in this study are retained in more general configurations. Secondly, while this work focuses on the impact of surface

viscous stresses, future research could explore more complex interfacial behaviors, including how surface viscous stresses, together with Marangoni stresses due to surface concentration inhomogeneity [20,47], influence propulsion behavior. Finally, a small-deformation analysis or numerical simulations examining the impacts of droplet deformability on the propulsion dynamics represents another direction for future studies. Overall, our findings represent a first step towards understanding how complexities arising from realistic biological or environmental systems impact the propulsion behaviors of active droplets driven by enclosed microswimmers, paving the way for their potential applications in these complex environments.

ACKNOWLEDGMENTS

APPENDIX A: COEFFICIENTS IN THE VELOCITY FIELD INTERIOR AND EXTERIOR TO THE DROPLET

The coefficients in the velocity field generated by a neutral squirmer, $\mathbf{u}_j^{\bar{B}_1}$, are given by

$$A_1 = \frac{2[b(1-\lambda) + \mathrm{Bq}_d]}{b^6(3\lambda + 2) + 2(b^5 - 1)\mathrm{Bq}_d + 2b(\lambda - 1)}, \tag{A1a}$$

$$B_1 = \frac{10b^2[b(\lambda - 1) - \mathrm{Bq}_d]}{b^6(9\lambda + 6) + 6(b^5 - 1)\mathrm{Bq}_d + 6b(\lambda - 1)}, \tag{A1b}$$

$$C_1 = 0, \tag{A1c}$$

$$D_1 = \frac{2b^5[b(3\lambda + 2) + 2\mathrm{Bq}_d]}{b^6(9\lambda + 6) + 6(b^5 - 1)\mathrm{Bq}_d + 6b(\lambda - 1)}, \tag{A1d}$$

$$E_1 = 0, \tag{A1e}$$

$$F_1 = \frac{10b^6\lambda}{b^6(9\lambda + 6) + 6(b^5 - 1)\mathrm{Bq}_d + 6b(\lambda - 1)}, \tag{A1f}$$

with other coefficients in Eqs. (8)–(11) being zero.

The coefficients in $\mathbf{u}_j^{\bar{B}_2}$ are given by

$$A_2 = \frac{2}{(b-1)^2 W_2}[-5b[(b^2 + b)(3b^2 + 2\lambda - 2) + 2(\lambda - 1)]$$
$$- 2(b - 1)(3b^3 + 6b^2 + 4b + 2)(3\mathrm{Bq}_d + 2\mathrm{Bq}_s)], \tag{A2a}$$

$$B_2 = \frac{2}{(b-1)^2 W_2}[5b[(b^2 + b)[5b^4 - 2b^2 + 2(b^4 + b^2 + 1)\lambda - 2] + 2(\lambda - 1)]$$
$$+ 2(b - 1)(5b^5 + 10b^4 + 8b^3 + 6b^2 + 4b + 2)(3\mathrm{Bq}_d + 2\mathrm{Bq}_s)], \tag{A2b}$$

$$C_2 = \frac{2b^3}{(b-1)^2 W_2}[5b\{b[-2(b^5 + b^4 + b^3 + b^2 + b)(\lambda + 1) - 2\lambda + 5] - 2\lambda + 5\}$$
$$- 2(b - 1)(2b^5 + 4b^4 + 6b^3 + 8b^2 + 10b + 5)(3\mathrm{Bq}_d + 2\mathrm{Bq}_s)], \tag{A2c}$$

$$D_2 = \frac{2b^5}{(b-1)^2 W_2}[5b\{b[2(b^3 + b^2 + b)(\lambda + 1) - 3] - 3\}$$
$$+ 2(b - 1)(2b^3 + 4b^2 + 6b + 3)(3\mathrm{Bq}_d + 2\mathrm{Bq}_s)], \tag{A2d}$$

$$E_2 = \frac{10\lambda b^4(3b^4 + 9b^3 + 11b^2 + 9b + 3)}{W_2}, \tag{A2e}$$

$$F_2 = -\frac{10\lambda b^6(3b^4 + 9b^3 + 11b^2 + 9b + 3)}{W_2}, \tag{A2f}$$

$$\begin{aligned}
W_2 = {} & 2(b - 1)(4b^6 + 16b^5 + 40b^4 + 55b^3 + 40b^2 + 16b + 4)(3\mathrm{Bq}_d + 2\mathrm{Bq}_s) \\
& + 5b[b[(4b^6 + 12b^5 + 24b^4)(\lambda + 1) + 30b^3\lambda + 15b^3 + 30b^2\lambda - 15b^2 \\
& + 24b(\lambda - 1) + 12(\lambda - 1)] + 4(\lambda - 1)],
\end{aligned} \tag{A2g}$$

with other coefficients in Eqs. (8)–(11) being zero.

APPENDIX B: EFFECT OF SWIMMING WITH A RADIAL SQUIRMING MODE

While previous studies have largely focused on squirmers with tangential surface velocities, we investigate the effect due to a radial squirming motion in this appendix and compare the results with those for a clean droplet scenario in Reigh *et al.* [14]. Similar to tangential squirming motion, among all modes of radial surface velocity distributions expressed as $\mathbf{u}_{\mathrm{sq}} = \sum_{n=0}^{\infty} \bar{A}_n P_n(\cos\theta)\mathbf{e}_r$, only a single mode (the $\bar{A}_1$ mode) contributes to swimming [23,24,33]. We therefore extend the analysis in the main text to include the effect due to the $\bar{A}_1$ mode. Specifically, under the same nondimensionalizations, the boundary condition for the radial component of the velocity on the squirmer surface, Eq. (12), becomes

$$u_{r,1}(r = 1) = (\alpha + U_S)\cos\theta, \tag{B1}$$

where $\alpha = \bar{A}_1/\bar{B}_1$ includes the effect due to the radial squirming mode. Following the same approach outlined in the main text, the propulsion speed of the squirmer is calculated as

$$\begin{aligned}
U_S = {} & \frac{1}{b^6(9\lambda + 6) + 6(b^5 - 1)\mathrm{Bq}_d + 6b(\lambda - 1)}\{2[6\alpha + (2 - \alpha)b^5 - 5(\alpha + 1)b^2 + 3]\mathrm{Bq}_d \\
& + (2 - \alpha)b^6(3\lambda + 2) + 2b[5(\alpha + 1)b^2 + 6(2\alpha + 1)](\lambda - 1)\},
\end{aligned} \tag{B2}$$

whereas the speed of the enclosing droplet is given by

$$U_D = \frac{10(\alpha + 1)b^3\lambda}{b^6(9\lambda + 6) + 6(b^5 - 1)\mathrm{Bq}_d + 6b(\lambda - 1)}. \tag{B3}$$

The speeds of both the squirmer and the droplet remain unaffected by surface shear viscosity (independent of Bq_s) when radial squirming motion is present. When $\alpha = 0$, the above results reduce to those with purely tangential squirming motion given by Eqs. (19) and (20) in the main text. A purely tangential squirmer consistently swims faster than its enclosing droplet ($U_D < U_S$). However, as indicated by Eq. (B3), incorporating radial squirming increases the droplet's speed, allowing the possibility of a coswimming state where the squirmer and droplet move at the same speed ($U_D = U_S$) in a concentric configuration [14].

The critical value, $\alpha = \alpha_C$, at which coswimming occurs can be determined as

$$\alpha_C = \frac{2[(2b^5 - 5b^2 + 3)\mathrm{Bq}_d + b[b^5(3\lambda + 2) - 5b^2 - 3\lambda + 3]]}{b^6(3\lambda + 2) + 10b^3 + 2(b^5 + 5b^2 - 6)\mathrm{Bq}_d + 12b(\lambda - 1)}, \tag{B4}$$

giving rise to a coswimming speed of

$$U_C = \frac{10b^3\lambda}{b^6(3\lambda + 2) + 10b^3 + 2(b^5 + 5b^2 - 6)\mathrm{Bq}_d + 12b(\lambda - 1)}. \tag{B5}$$

The above results reduce to the case of a clean droplet [14] when $\mathrm{Bq}_d = 0$. Equation (B5) shows that surface dilatational viscosity causes a monotonic reduction in the coswimming speed.

[1] A. D. Griffiths and D. S. Tawfik, Miniaturising the laboratory in emulsion droplets, Trends Biotechnol. **24**, 395 (2006).

[2] B. T. Kelly, J.-C. Baret, V. Taly, and A. D. Griffiths, Miniaturizing chemistry and biology in microdroplets, Chem. Commun. **2007**, 1773 (2007).

[3] M. He, J. S. Edgar, G. D. M. Jeffries, R. M. Lorenz, J. P. Shelby, and D. T. Chiu, Selective encapsulation of single cells and subcellular organelles into picoliter- and femtoliter-volume droplets, Anal. Chem. **77**, 1539 (2005).

[4] M. Chabert and J.-L. Viovy, Microfluidic high-throughput encapsulation and hydrodynamic self-sorting of single cells, Proc. Natl. Acad. Sci. USA **105**, 3191 (2008).

[5] J. Clausell-Tormos, D. Lieber, J.-C. Baret, A. El-Harrak, O. J. Miller, L. Frenz, J. Blouwolff, K. J. Humphry, S. Köster, H. Duan, C. Holtze, D. A. Weitz, A. D. Griffiths, and C. A. Merten, Droplet-based microfluidic platforms for the encapsulation and screening of mammalian cells and multicellular organisms, Chem. Bio. **15**, 427 (2008).

[6] H. Wen, Y. Yu, G. Zhu, L. Jang, and J. Qin, A droplet microchip with substance exchange capability for the developmental study of *C. elegans*, Lab Chip **15**, 1905 (2015).

[7] W. Gao and J. Wang, The environmental impact of micro/nanomachines: A review, ACS Nano **8**, 3170 (2014).

[8] J. Li, B. E.-F. de Ávila, W. Gao, L. Zhang, and J. Wang, Micro/nanorobots for biomedicine: Delivery, surgery, sensing, and detoxification, Sci. Robot. **2**, eaam6431 (2017).

[9] C. K. Schmidt, M. Medina-Sánchez, R. J. Edmondson, and O. G. Schmidt, Engineering microrobots for targeted cancer therapies from a medical perspective, Nat. Commun. **11**, 5618 (2020).

[10] Z. Wu, Y. Chen, D. Mukasa, O. S. Pak, and W. Gao, Medical micro/nanorobots in complex media, Chem. Soc. Rev. **49**, 8088 (2020).

[11] B. J. Nelson and S. Pané, Delivering drugs with microrobots, Science **382**, 1120 (2023).

[12] R. Nauber, S. R. Goudu, M. Goeckenjan, M. Bornhäuser, C. Ribeiro, and M. Medina-Sánchez, Medical microrobots in reproductive medicine from the bench to the clinic, Nat. Commun. **14**, 728 (2023).

[13] Y. Ding, F. Qiu, X. C. Solvas, F. W. Y. Chiu, B. J. Nelson, and A. DeMello, Microfluidic-based droplet and cell manipulations using artificial bacterial flagella, Micromachines **7**, 25 (2016).

[14] S. Y. Reigh, L. Zhu, F. Gallaire, and E. Lauga, Swimming with a cage: low-reynolds-number locomotion inside a droplet, Soft Matter **13**, 3161 (2017).

[15] R. Kree, L. Rückert, and A. Zippelius, Dynamics of a droplet driven by an internal active device, Phys. Rev. Fluids **6**, 034201 (2021).

[16] K. V. S. Chaithanya and P. T. Sumesh, Deformation dynamics of an active compound particle in an imposed shear flow—a theoretical study, J. Phys. D: Appl. Phys. **53**, 314001 (2020).

[17] G. G. Fuller and J. Vermant, Complex fluid-fluid interfaces: Rheology and structure, Annu. Rev. Chem. Biomol. Eng. **3**, 519 (2012).

[18] J. R. Samaniuk and J. Vermant, Micro and macrorheology at fluid–fluid interfaces, Soft Matter **10**, 7023 (2014).

[19] N. O. Jaensson, P. D. Anderson, and J. Vermant, Computational interfacial rheology, J. Non-Newtonian Fluid Mech. **290**, 104507 (2021).

[20] V. A. Shaik, V. Vasani, and A. M. Ardekani, Locomotion inside a surfactant-laden drop at low surface Péclet numbers, J. Fluid Mech. **851**, 187 (2018).

[21] A. R. Sprenger, V. A. Shaik, A. M. Ardekani, M. Lisicki, A. J. T. M. Mathijssen, F. Guzmán-Lastra, H. Löwen, A. M. Menzel, and A. Daddi-Moussa-Ider, Towards an analytical description of active microswimmers in clean and in surfactant-covered drops, Eur. Phys. J. E **43**, 58 (2020).

[22] V. A. Shaik and A. M. Ardekani, Point force singularities outside a drop covered with an incompressible surfactant: Image systems and their applications, Phys. Rev. Fluids **2**, 113606 (2017).

[23] M. J. Lighthill, On the squirming motion of nearly spherical deformable bodies through liquids at very small Reynolds numbers, Commun. Pure Appl. Math. **5**, 109 (1952).

[24] J. R. Blake, A spherical envelope approach to ciliary propulsion, J. Fluid Mech. **46**, 199 (1971).

[25] T. J. Pedley, Spherical squirmers: Models for swimming micro-organisms, IMA J. Appl. Math. **81**, 488 (2016).

[26] T. Ishikawa, Fluid dynamics of squirmers and ciliated microorganisms, Annu. Rev. Fluid Mech. **56**, 119 (2024).

[27] S. Kim and S. J. Karrila, *Microhydrodynamics: Principles and Selected Applications* (Dover, New York, 1991).

[28] J. Happel and H. Brenner, *Low Reynolds Number Hydrodynamics: With Special Applications to Particulate Media* (Noordhoff International Publishing, Leyden, 1973).

[29] L. E. Scriven, Dynamics of a fluid interface, Chem. Eng. Sci. **12**, 98 (1960).

[30] L. G. Leal, *Advanced Transport Phenomena: Fluid Mechanics and Convective Transport Processes* (Cambridge University Press, Cambridge, 2007).

[31] R. S. Subramanian and R. Balasubramaniam, *The Motion of Bubbles and Drops in Reduced Gravity* (Cambridge University Press, Cambridge, 2001).

[32] H. Lamb, *Hydrodynamics* (Cambridge University Press, Cambridge, 1932).

[33] O. S. Pak and E. Lauga, Generalized squirming motion of a sphere, J. Eng. Math. **88**, 1 (2014).

[34] S. Y. Reigh and E. Lauga, Two-fluid model for locomotion under self-confinement, Phys. Rev. Fluids **2**, 093101 (2017).

[35] H. Nganguia, L. Zhu, D. Palaniappan, and O. S. Pak, Squirming in a viscous fluid enclosed by a Brinkman medium, Phys. Rev. E **101**, 063105 (2020).

[36] S. K. Agrawal and D. T. Wasan, The effect of interfacial viscosities on the motion of drops and bubbles, J. Chem. Eng. **18**, 215 (1979).

[37] M. D. Levan, Motion of a droplet with a Newtonian interface, J. Colloid Interface Sci. **83**, 11 (1981).

[38] V. Narsimhan, Letter: The effect of surface viscosity on the translational speed of droplets, Phys. Fluids **30**, 081703 (2018).

[39] L. M. C. Sagis, Dynamic properties of interfaces in soft matter: Experiments and theory, Rev. Mod. Phys. **83**, 1367 (2011).

[40] A. Andersen, J. Oertegren, P. Koelsch, D. Wantke, and H. Motschmann, Oscillating bubble SHG on surface elastic and surface viscoelastic systems: New insights in the dynamics of adsorption layers, J. Phys. Chem. B **110**, 18466 (2006).

[41] J. Maldonado-Valderrama, V. B. Fainerman, M. J. Gálvez-Ruiz, A. Martín-Rodriguez, M. A. Cabrerizo-Vílchez, and R. Miller, Dilatational rheology of β-casein adsorbed layers at liquid-fluid interfaces, J. Phys. Chem. B **109**, 17608 (2005).

[42] M. Lakshmanan, A. Dhathathreyan, and R. Miller, Synergy between hofmeister effect and coupled water in proteins: Unusual dilational moduli of BSA at air/solution interface, Colloids Surf. A **324**, 194 (2008).

[43] F. Monroy, H. M. Hilles, F. Ortega, and R. G. Rubio, Relaxation dynamics of langmuir polymer films: A power-law analysis, Phys. Rev. Lett. **91**, 268302 (2003).

[44] H. Hilles, F. Monroy, L. J. Bonales, F. Ortega, and R. G. Rubio, Fourier-transform rheology of polymer langmuir monolayers: Analysis of the non-linear and plastic behaviors, Adv. Colloid Interface Sci. **122**, 67 (2006).

[45] M. Vrânceanu, K. Winkler, H. Nirschl, and G. Leneweit, Surface rheology and phase transitions of monolayers of phospholipid/cholesterol mixtures, Biophys. J. **94**, 3924 (2008).

[46] L. R. Arriaga, I. López-Montero, J. Ignés-Mullol, and F. Monroy, Domain-growth kinetic origin of nonhorizontal phase coexistence plateaux in Langmuir monolayers: Compression rigidity of a raft-like lipid distribution, J. Phys. Chem. B **114**, 4509 (2010).

[47] R. Dandekar and A. M. Ardekani, Effect of interfacial viscosities on droplet migration at low surfactant concentrations, J. Fluid Mech. **902**, A2 (2020).